Equivalent Force Extraction Methodology for Electrical Component Induced PCB Vibration

Yifan Ding , *Graduate Student Member, IEEE*, Jianmin Zhang, *Senior Member, IEEE*, Ming-Feng Xue , Xin Hua, Benjamin Leung, Eric A. MacIntosh, *Member, IEEE*, and Chulsoon Hwang, *Senior Member, IEEE*

Abstract—On-board electrical components can cause printed circuit board (PCB) vibration, thus generating audio noise if the electrical noise is in the audible frequency range. The electrical component-induced vibration can be equated to an external force applied to the PCB. This article presents a novel methodology to extract the equivalent force of electrical components on a PCB to study board vibration and potential acoustic noise problems. The method is based on a combination of measurement and simulation, wherein PCB vibration is used as the medium in the extraction process. The methodology is validated by the correlation of PCB vibration pattern, frequency, and amplitude with a known electromagnetic force applied to the PCB.

Index Terms—Electromagnetic force, force extraction methodology, harmonic analysis, laser doppler vibrometer (LDV), modal analysis, printed circuit board (PCB) vibration.

I. Introduction

7 ITH the development of electronic technology and the increasing requirements for the stability of electronic products, printed circuit boards (PCBs) have been well studied in terms of electrical performance, including signal integrity, power integrity, and electromagnetic compatibility (EMC). Channel loss [1], crosstalk [2], [3], and impedance control [4] are the three major areas associated with PCB signal integrity, and the low impedance power distribution network (PDN) [5], [6] is the main topic of PCB power integrity. Regarding electromagnetic compatibility analysis and modeling, equivalent source model reconstruction is the most interesting subject for far-field radiation emission prediction [7], [8] and near-field coupling analysis such as radio frequency desense [9]. Beyond electrical performance studies, the heat dissipation performance of a PCB has been analyzed [10], and thermal-associated stress, deformation, and thermal-force coupling have been studied [11].

Not only the electrical performance but also mechanical behavior should be considered. Unwanted board vibration causes

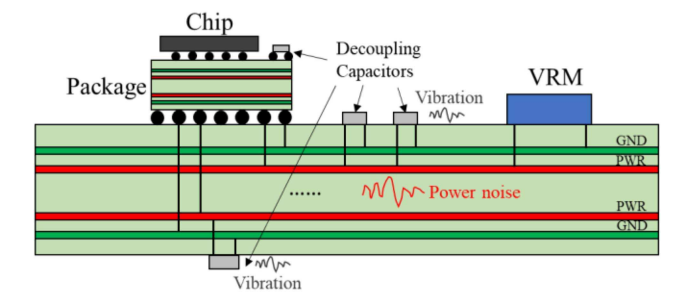
Manuscript received 16 March 2023; revised 19 July 2023 and 1 September 2023; accepted 17 September 2023. Date of publication 3 October 2023; date of current version 16 February 2024. This work was supported in part by the National Science Foundation (NSF) under Grant IIP-1916535. (Corresponding author: Chulsoon Hwang.)

Yifan Ding and Chulsoon Hwang are with the EMC Laboratory, Missouri University of Science and Technology, Rolla, MO 65401 USA (e-mail: dingyif@mst.edu; hwangc@mst.edu).

Jianmin Zhang, Ming-Feng Xue, Xin Hua, Benjamin Leung, and Eric A. MacIntosh are with the Google LLC, Mountain View, CA 94043 USA (e-mail: jianmin@google.com; mingfengx@google.com; xihua@google.com; benleung@google.com; ericmac@google.com).

Color versions of one or more figures in this article are available at https://doi.org/10.1109/TEMC.2023.3319272.

Digital Object Identifier 10.1109/TEMC.2023.3319272



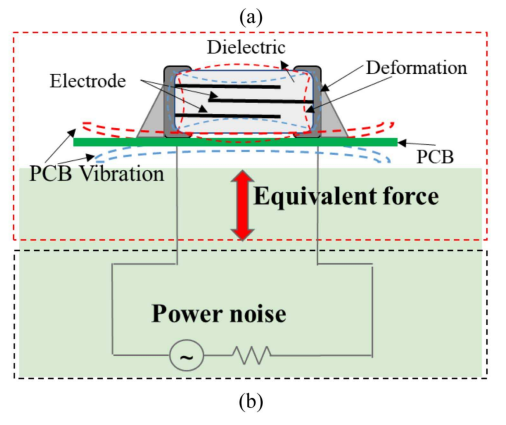


Fig. 1. (a) PDN power rail noise caused electrical component vibration. (b) Example of an electrical component–MLCC deformation and the equivalent force caused PCB vibration.

fatigue damage to electrical systems and generates acoustic noise if the vibration is in the audible frequency range. A prior study [12] has described the analysis of PCB dynamic characteristics subjected to vibration loadings under various clamping conditions. The fatigue life of electronic equipment from the board level under random vibration situations has also been predicted [13] by considering the structure and external excitation. PCB electrical behavior and mechanical behavior are not independent of each other. The selection of the electrical components and board layout design can also affect the mechanical performance of PCBs. For example, the power supply noise can be transferred to the mechanical moment on the electrical components, such as multilayer ceramic capacitors (MLCCs), owing to the piezoelectric effect, as shown in Fig. 1(a). If the noise frequency is in the audible frequency range, the resultant PCB vibration is likely to produce audio noise. When the noise frequency is aligned with the PCB self-resonant frequency, and the excitation source is located at the area with large self-resonance

0018-9375 \odot 2023 IEEE. Personal use is permitted, but republication/redistribution requires IEEE permission. See https://www.ieee.org/publications/rights/index.html for more information.

deformations, the PCB vibration velocity will be large and the corresponding acoustic noise at that frequency will be hearable. The magnitude of the acoustic noise is typically measured using the sound pressure level (SPL) [14]. This acoustic noise can degrade user experience with mobile devices, particularly in products such as earbuds and smartphones. Other electronic components, such as the inductors in dc–dc converters, can also create vibration due to the magnetostrictive effect.

Electromagnetic field and force can be coupled together. For example, when a current-carrying wire is placed within a magnetic field, each of the moving charges experiences the Lorentz force. In the cases stated in the previous paragraph, when the electrical components such as the multilayer ceramic capacitors and the inductors that have piezoelectric effect or magnetostrictive effect are powered ON, the power noise will cause the deformation of the components. Since the components are soldered or mounted on the PCB, the interior deformation of the electrical component will output force to the PCB through the soldering pad or mounting fixture, which is described in Fig. 1(b), and the equivalent force will cause the PCB to vibrate and generate acoustic noise.

Quantification of the equivalent force generated by an electrical component under a given voltage/current condition is desirable. A PCB, loaded by components and mounted on a supporting base, is a mechanical system with a characteristic system response. The equivalent force from each component can be regarded as a mechanical excitation. In most cases, the force is sufficiently small, and the PCB mechanical system can be regarded as linear. Therefore, harmonic analysis at each frequency point can be performed to calculate the amplitude of board vibration when multiple electrical components are excited. This practice can be further extended to the optimization of component placement, trace routing, and board fixture point selection.

Quantitative studies of the equivalent mechanical force generated by on-board electrical components have rarely been reported in the literature. Because the force from a vibrating electrical component is weak and tiny, directly measuring (e.g., using an accelerometer) is very challenging and accuracy cannot be guaranteed. Recently, a fully controllable electromagnetic force has been proposed to mimic the mechanical behavior of the on-PCB electrical component [15]. PCB vibrations are effectively excited, and the same board behavior is observed when an electrical component, e.g., MLCC, is excited. Thus, the equivalent force of an electrical component on the PCB can potentially be determined by matching the PCB vibration amplitude caused by the electrical component and that excited by a given mechanical force at each frequency.

Herein, a systematic and efficient methodology is proposed for the first time to extract and characterize the equivalent force generated by the electrical components on the PCB. This methodology relies on the measurement, simulation, and deembedding of the PCB vibration velocity at the resonance frequency after applying the external force. The proposed methodology was validated by using the electromagnetic force from the coil—magnet system that can be obtained through direct simulation, also extracted from the proposed force extraction

flow. The forces from the two methods matched well, with a discrepancy of 11%, thus validated the force extraction method.

The basic theory for solving the vibration problem is described in Section II. The on-PCB electrical component mechanical force extraction methodology is presented in Section III. In Section IV, the mechanical force extraction methodology is validated by using a force produced according to the mutual effect between a magnet and a coil with ac current. Conclusions are discussed in Section V.

II. ANALYSIS OF PCB VIBRATION CAUSED BY ELECTRICAL COMPONENTS

In this section, the mechanical behavior and equivalent force of the electrical components on a PCB are identified. The fundamental theory of the PCB vibration problem is reviewed for completeness.

A. Force From on-PCB Electrical Components

The equivalent force under study interacts with the board platform rather than standing alone in the free status. The work herein focuses on the situation in which the electrical component is soldered on the PCB.

The equivalent force of a single electrical component is small and cannot be directly measured by traditional force sensors, e.g., accelerometers, with acceptable accuracy. Therefore, the electrical component force extraction strategy relies on the PCB vibration caused by the component, which can be measured by a laser Doppler vibrometer (LDV) with an accuracy of 0.01 nm/s. As such, the problem of finding the force is converted to the problem of measuring PCB vibration amplitude. Notably, although the PCB is used as the medium for the equivalent force extraction, the force is part of the electrical component characteristics but not of the PCB.

B. General Equation of Motion

An external force loaded into a system will cause the system vibration and deformation. The relationships among the system, external force, and the effect of the force is expressed in (1) by using the general equation of motion [16]. If a force $\{F(t)\}$ is loaded, it can be decomposed into three terms: the force for inertia F_{inertia} , equal to $[M]\{\ddot{u}\}$; the force for damping F_{damping} , which is written as $[C]\{\dot{u}\}$; and the force for stiffness $F_{\text{stiffness}}$, which is given by $[K]\{u\}$

$$[M] \{\ddot{u}\} + [C] \{\dot{u}\} + [K] \{u\} = \{F(t)\}$$
 (1)

where

[M] is the structural mass matrix;

[C] is the structural damping matrix;

[K] is the structural stiffness matrix;

 $\{F\}$ is the load vector;

 $\{\ddot{u}\}$ is the nodal acceleration vector;

 $\{\dot{u}\}$ is the nodal velocity vector;

 $\{u\}$ is the nodal displacement vector;

(t) is the time.

With the above equation, the force can be calculated as follows: mass, damping, and stiffness can be obtained from the design, whereas acceleration, velocity, and displacement can be obtained from the LDV measurement. All the variables are known, thus enabling the loaded force vector to be obtained with this method.

C. PCB Self-Resonance

For a PCB with a regular shape, an analytical solution of the vibration modes exists. In the following example, the PCB can be regarded as a rectangular plate in the x-y plane. In a prior study [17], another format of the out-of-plane displacement is given when an external load is forced on the PCB. In the situation in which no force is applied to the structure, the intrinsic vibration can be solved with the following equation:

$$\frac{Eh^3}{12\left(1-v^2\right)}\left(\frac{\partial^4\omega}{\partial x^4}+2\frac{\partial^4\omega}{\partial x^2\partial y^2}+\frac{\partial^4\omega}{\partial y^4}\right)+\gamma\frac{\partial^2\omega}{\partial t^2}=0\quad (2)$$

where E is Young's modulus, v is Poisson's ratio, h is the plate thickness, t is time, and γ is the mass per unit area.

The modal solution of (2) for a rectangular plate with length a and width b is given by (3) with $\omega(x, y, t) = \phi(x, y)T(t)$, as follows:

$$\phi_{ij}(x,y) = \sin\left(\frac{i\pi x}{a}\right) \sin\left(\frac{i\pi y}{b}\right)$$
 (3)

where i and j are modal indices denoting the number of half waves in the mode shape along the x and y coordinates, respectively. The corresponding natural frequency is expressed as follows:

$$f_{ij} = \frac{1}{2\pi} \left[\left(\frac{i\pi}{a} \right)^2 + \left(\frac{j\pi}{b} \right)^2 \right] \sqrt{\frac{Eh^3}{12\gamma \left(1 - v^2 \right)}}.$$
 (4)

The modal solutions including the mode pattern and the resonance frequency are critical for identifying the PCB vibration. For example, for a four-layer PCB with eight fixing holes, when the left top and right bottom corner of the board is fixed, the PCB self-resonance mode deformations without any excitations are shown in Fig. 2. For different boundary conditions, the mode pattern and resonance frequencies can differ.

In the following sections, the PCB vibration velocity amplitude is measured and simulated in the frequency and space domains. From the frequency perspective, focusing on narrow bands around each resonant frequency of the PCB is reasonable, because vibration at resonance has a larger amplitude and a more distinguished pattern than that at other frequencies. From the space perspective, the PCB vibration can vary among locations for each resonance mode. At each resonant frequency, because the vibration velocity is the first-order derivative of the deformation with respect to time, the larger deformation means the larger vibration velocity at that location. Therefore, based on the deformation patterns, locations with large vibration amplitude can be selected as sample points for the purpose of force extraction.

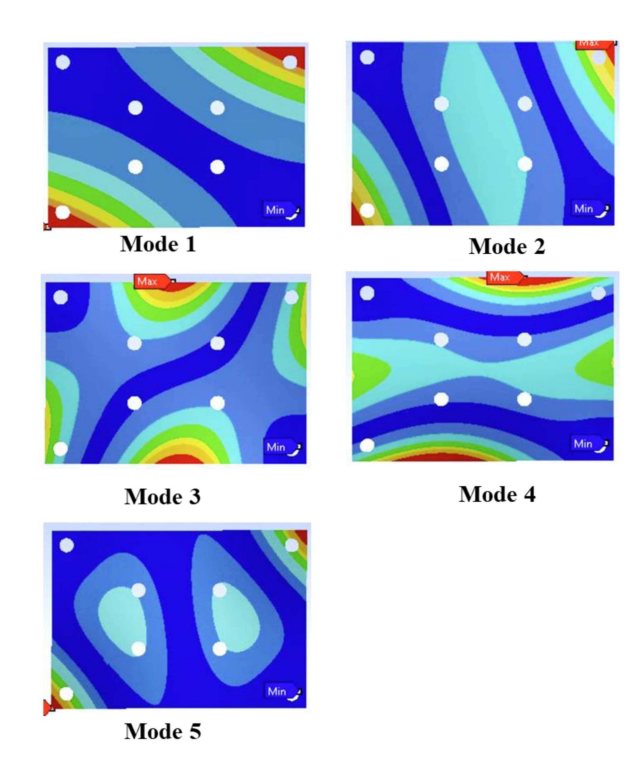


Fig. 2. Focused mode deformation pattern examples of a PCB with the boundary condition of two fixed points at the left top and right bottom corner.

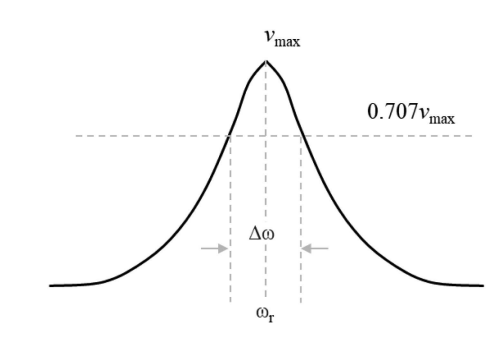


Fig. 3. Half-power method for damping ratio calculation.

D. Damping Ratio

In a real system, friction will damp the system vibration and dissipate energy. The system oscillation after a disturbance is described by using the quantity of damping ratio. The damping ratio must be considered in the structure simulation to correctly mimic the vibration of the system.

The system damping ratio can be obtained through many methods. In a prior study [18], a frequency domain interpolation method for the estimation of the damping ratio, which is necessary for structure dynamic analysis, has been presented. The two conventional techniques—the random decrement method and the half-power method—have been described and compared [19]. The efficiency and accuracy of the methods have been verified. Because the methodology proposed herein focuses on the behavior of the system resonance frequencies, the half-power method given in (5) and shown in Fig. 3 is used for estimating

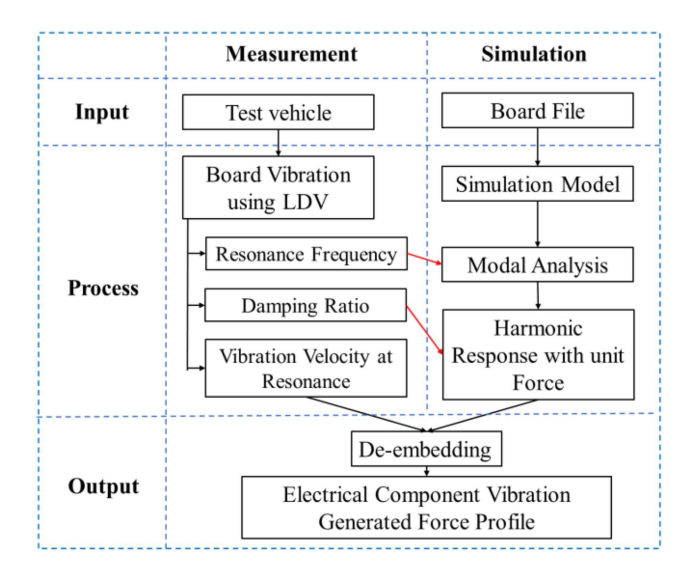


Fig. 4. Extraction methodology for the force caused by electrical component vibration.

damping, on the basis of finding the bandwidth of each mode

$$\gamma = \frac{\Delta\omega}{2\omega_r} \tag{5}$$

where $\Delta\omega$ is the absolute bandwidth of the resonant response at the amplitude of 0.707 $v_{\rm max}$ and ω_r is the resonance frequency.

III. ELECTRICAL COMPONENT MECHANICAL FORCE EXTRACTION METHODOLOGY

This section introduces a novel mechanical force extraction methodology that relies on measurement and simulation. This hybrid method was inspired by prior studies [20], [21] reporting the simulation and measurement methodology for the PCB vibration, and a study [22] proposing an automatic simulation flow. The PCB vibration velocity caused by the mechanical force is the critical quantity to be measured and compared with the simulation. The force extraction methodology is shown in Fig. 4.

The procedures of the methodology are described in detail below.

A. Measurement Process

The input and process of the measurement is as follows.

- 1) The device under test (DUT), which is the input of the measurement, is the PCB with a given boundary condition and the component under test with the given electrical input as the excitation.
- 2) The LDV is used to measure the board vibration caused by component deformation and vibration.
- 3) Three quantities are measured in this process:
 - a) The mode resonance frequency of the PCB, used to verify whether the simulation model is accurate
 - b) The damping ratio, obtained from the measurement using the half-power method in (5) and used in the simulation to mimic the actual behavior of the PCB.

c) The PCB vibration velocities at the mode resonance frequencies.

B. Simulation Process

The input and process of the simulation is as follows.

- 1) The input of the simulation process is a simulation model converted from the PCB board file. The simulation tool used in this process is Ansys Mechanical.
- 2) The material properties of the PCB model are defined on the basis of the real design. Boundary conditions are also defined to be consistent with the measurement setup. The mesh settings including the mesh type and mesh size to achieve the convergence of the mode resonance frequencies that will be obtained in the next step.
- 3) Modal analysis is first performed to obtain the PCB mode resonance frequencies. The frequencies and the mode pattern are compared with the measurements to demonstrate the accuracy of the model.
- 4) The damping ratio extracted from the measurement for different frequencies is defined in the simulation setup. The unit force of 1 μ N is applied to the PCB model at the same location of the vibrated electrical component on the measurement DUT to perform harmonic response analysis.
- 5) The output of the harmonic response analysis is the board vibration velocity at different resonant frequencies.

C. De-Embedding Process

Two velocities, one from the measurement and caused by the electrical component vibration, and the other from the simulation and caused by the applied unit force, can be obtained after completion of the above steps. If the two forces from different sources are applied at the same location with the same amplitude and injection angle, the resultant PCB vibration velocity will have the same pattern and amplitude. The PCB vibration velocity is obtained through the test-vehicle PCB, but the force that causes the PCB vibration is independent of the PCB and only related to the nature of the electrical component itself and the electrical excitation. The process of extracting the force generated by the electrical component is essentially a process of removing the influence of the test-vehicle PCB embedded in the measured and simulated vibration velocity. Also, because the equivalent force is small and the system is linear, the PCB vibration velocity is proportional to the magnitude of the force applied. So, the equivalent force F_{eq} extracted through the velocity de-embedding is basically to find the ratio of the measured velocity over the simulated velocity in the following:

$$F_{\rm eq} = \frac{v_m}{v_s} \times F_{\rm unit} \tag{6}$$

where v_m is the measured PCB vibration velocity excited by the electrical component with a given input at the observation point, v_s is the simulated PCB vibration velocity excited by the unit force at the same location, and $F_{\rm unit}$ is the unit force applied in the simulation.

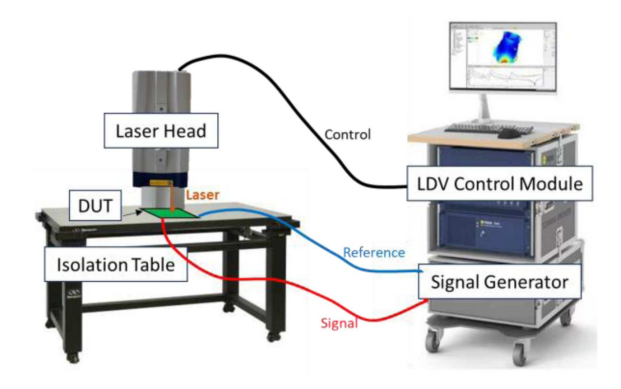


Fig. 5. Overview of the measurement setup.

The force profile for the target electrical component in a wide frequency range can be obtained by repeating the above process for different resonance frequencies. For the case of multiple electrical components mounted on the PCB, instead of extracting their equivalent force all together, the equivalent force of each component one can be extracted individually, and the linear system superposition law can be used to calculate the board vibration as an entire system. Another advantage of this methodology is that arbitrary combination of source magnitude and phase can be done in post-processing stage.

IV. VALIDATION OF THE FORCE EXTRACTION METHODOLOGY

To validate the force extraction methodology, an electromagnetic force from paper [15] whose value is controllable and knowable was used to test its accuracy. The measurement and simulation setups described below were used to validate the proposed force extraction methodology.

A. Measurements

The real measurement setup for the PCB vibration measurement is shown in Fig. 5. The LDV was controlled by the control module for laser positioning and signal input. The DUT was placed on the isolation table within the range of the laser point to isolate the vibration from the floor. Electrical input for the DUT, including the PCB and the on-PCB electrical components, such as capacitors, was from the system signal generator built in the LDV control module.

The DUT for the validation is the medium PCB with a size of 40 mm \times 57 mm that is shown in Fig. 6(a). The contained multiple power domains, and several capacitor soldering pads were connected to different power domains. Capacitors can be soldered on the pads, and the external force used for validation can also be applied to the same location of the capacitor. The test-vehicle PCB used for extracting the force was a commonly used four-layer PCB with simple structure and FR-4 material. Simpler PCB structure had smaller influence on the process of force extraction, because the structure was easy to model in the simulation. Thus, higher accuracy of the extracted force could be achieved. Furthermore, the PCB in this study was carefully selected to generate appropriate resonance frequencies and mode

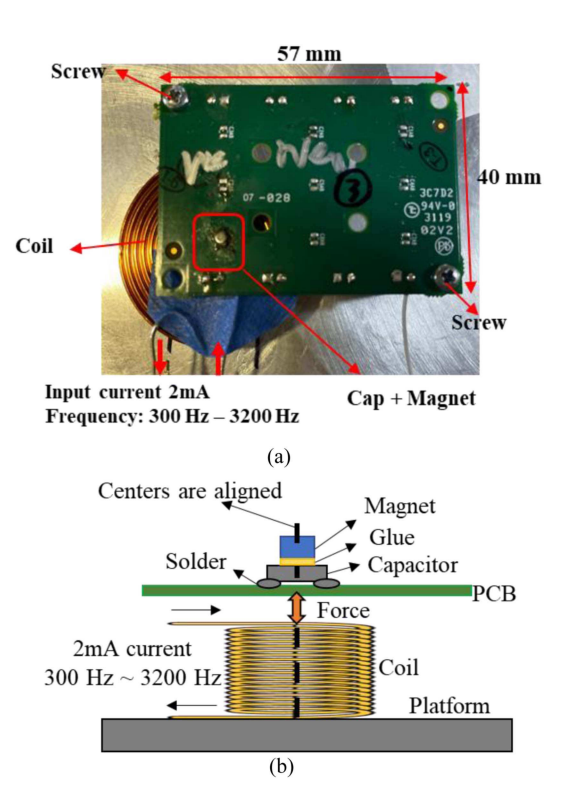


Fig. 6. Validation PCB with the electrical source of the mechanical force. (a) Top view of the measurement setup, showing the location of the applied force. (b) Side view schematic of the component arrangement.

patterns. With the given PCB size, the resonance frequencies of the first several modes of the test-vehicle PCB covered the targeted acoustic frequency range (300–3200 Hz).

The side view of the DUT layout is given to provide details of the component arrangement. As shown in Fig. 6(b), a capacitor in 0805 package size was soldered on the pads at the lower left corner of the PCB with no power input to the corresponding power rail. Therefore, the capacitor did not have moment caused by the piezoelectric effect. Apart from the pressure caused by the mass of the capacitor, the capacitor did not exert additional force on the PCB. A magnet with similar cross-sectional size of the capacitor was glued to the top surface of the capacitor. A coil was placed under the PCB at the platform where the PCB was fixed, and the centers of the coil and the magnet were well aligned vertically. A constant ac current with 2 mA amplitude was input to the coil for the frequency range from 300 to 3200 Hz, causing the PCB to vibrate following the same frequency. The external force to the system used for the methodology validation was from the mutual effect between the coil and magnet. Because the centers of the two components were aligned, the loaded electromagnetic force to the PCB system was in the vertical direction only. A total of eight mounting holes were designed for fixing the PCB with screws. In this example, two holes at the left top and right bottom corners were used for screw installation as the fixed boundary condition. The location of the excitation and the fixed boundary conditions were limited by the size of the coil. Also, a location where it is easy to excite the PCB vibration is selected.

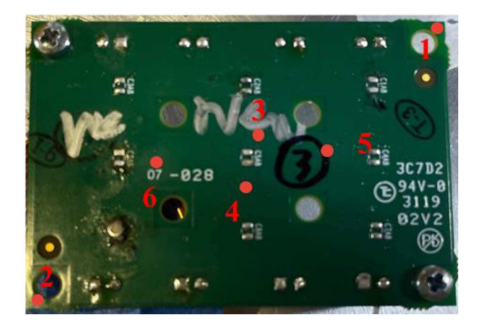


Fig. 7. Schematic of the observation points to decrease measurement error.

TABLE I
PCB SELF-RESONANCE FREQUENCY (Hz) COMPARISON FOR THE
TWO-FIXED-POINT BOUNDARY CONDITION

Mode	Measurement	Simulation	Δ
1	390.25	417.93	7.09%
2	1212	1173	3.22%
3	1558.125	1590.1	2.05%
4	2147.5	2095.5	2.42%
5	2817	2674.3	5.07%

In the measurement, 20 averages were used to average out the run-to-run variations in measurement. The frequency step was set to 0.25 Hz to capture the velocity point at the resonance as accurately as possible. On the basis of the dimensions of the board. Within the frequency range of interest, five resonance modes shown in Fig. 2 were investigated.

The six points on the PCB at different locations, as shown in Fig. 7, were selected as sample points to observe the resonance frequency, the damping ratio, and the board vibration velocity at the all the focused resonance modes. As presented in Fig. 2, the PCB vibration pattern and velocity at different locations and different frequencies varied. It is desirable to choose those with large vibration amplitude to make sure higher SNR and better measurement accuracy. However, for different modes, the location with maximum vibration varies. Capturing the maximum-vibration locations helps to improve accuracy but is also time-consuming considering the size of the test PCB. Besides, it is not easy to locate the maximum-vibration locations of all resonance frequencies. Due to the inevitable measurement uncertainty, maximum-vibration locations in the actual measurement may not be perfectly aligned with the simulation. As a practical strategy, six points where the vibration at each mode is not particularly small were selected. Given the limitations of measurement accuracy, the results measured at the observation points might have uncertainties. By taking the average of the resonance frequency and the damping ratio, the uncertainty from the observation locations was effectively decreased.

The resonance frequencies shown in Table I were obtained from the velocity response curve and the measured board deformation pattern in Fig. 8, which is a criterion for the accuracy of the simulation model. From (5), the damping ratios for the six selected observation points were extracted for the first five mode resonance frequencies. The damping ratio for the PCB, determined by averaging the damping ratios from the six observation

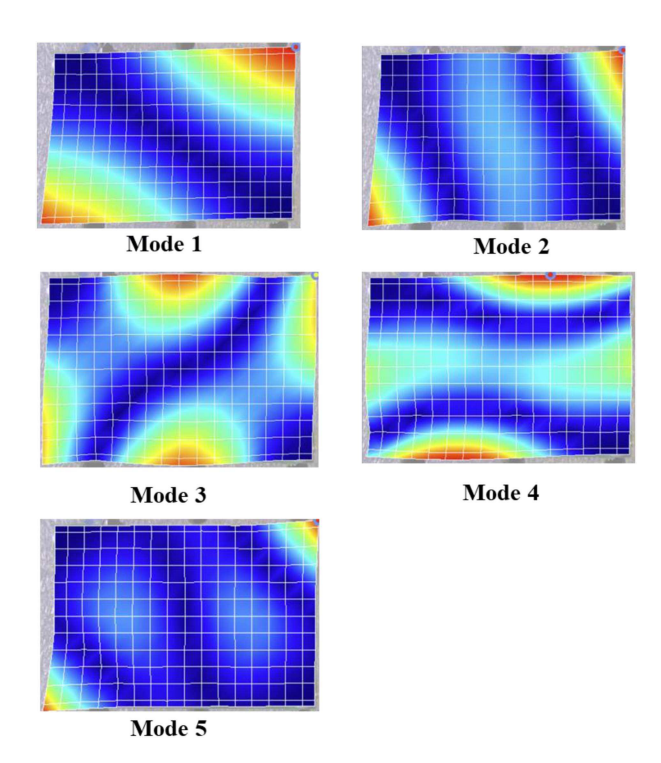


Fig. 8. Measured mode patterns of a PCB with the boundary condition of two fixed points at the left top and right bottom corner.

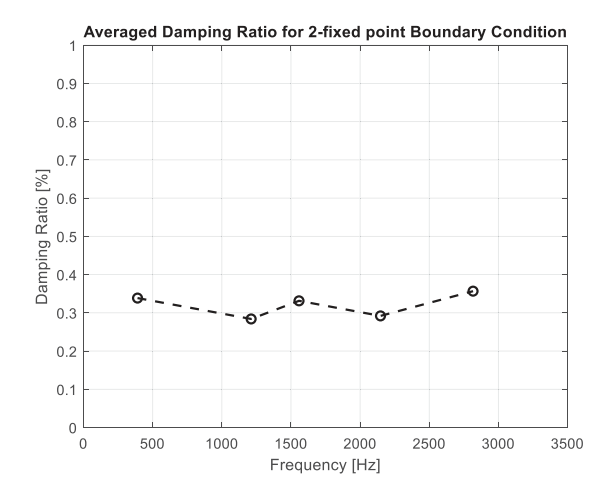
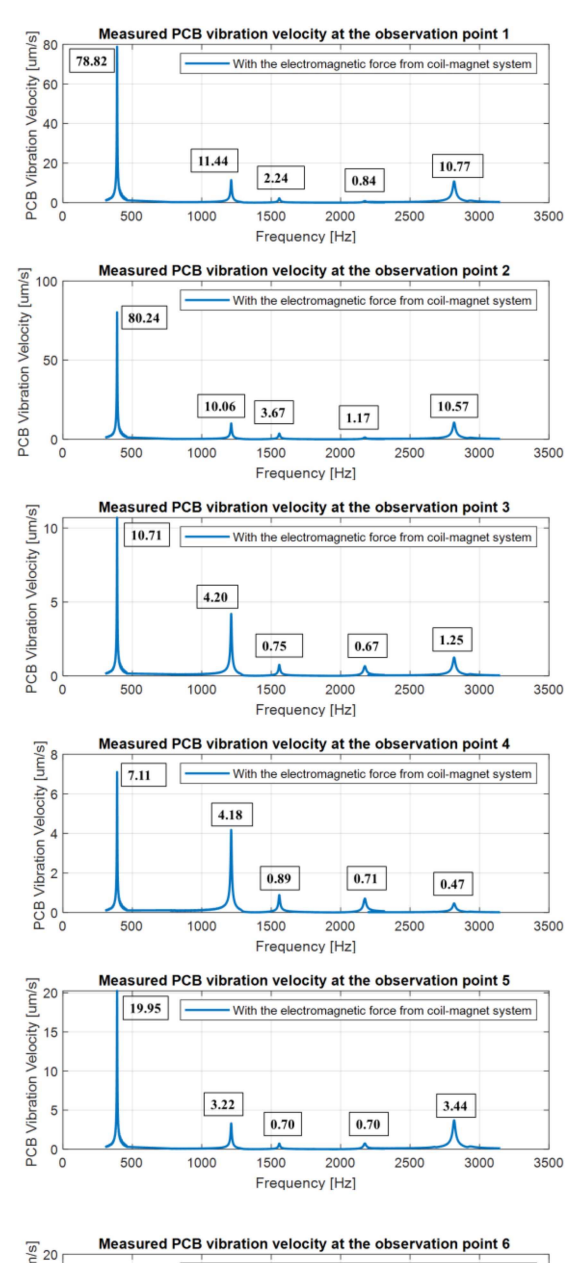


Fig. 9. PCB damping ratio after averaging all observation points for each mode.

points, is shown in Fig. 9. With 2 mA amplitude ac input current to the coil at each frequency, the board vibration velocities at the six observation points were also measured. The measured PCB vibration velocity response at the six observation points are shown in Fig. 10 as an example. The numbers noted in the figure are the vibration velocities at the resonance frequencies. A total of six velocity response curves from the six observation points were obtained for the focused modes, which were used in the de-embedding process.

B. Simulation

The simulation model was built in Ansys Mechanical by importing the PCB design file. To simplify the problem, each



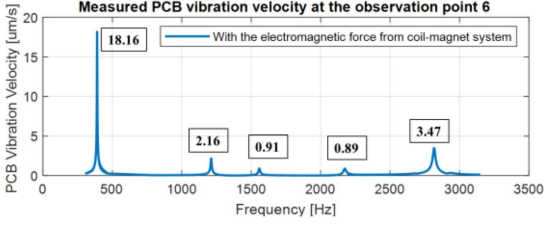


Fig. 10. Measured PCB vibration velocity at the observation point 1–6. The vibration is excited by the electromagnetic force from the coil-magnet system.

signal layer was considered a solid plane with a material formed by a mixture of copper and dielectric material in different ratios, to account for different trace routing situations. The material properties for the equivalent mass density, the coefficient of thermal expansion (CTE $_{xy}$ for in-plane and CTE $_z$ for out-of-plane), and Young's modulus (E_{xy} for in-plane and E_z for out-of-plane) were extracted from the PCB design file in Ansys Sherlock.

Layer	Туре	Material	Thickness
1	SIGNAL	COPPER (78.5%) / COPPER-RESIN	50.8 μm
2	Laminate	Generic FR-4	138.18 μm
3	SIGNAL	COPPER (82.8%) / COPPER-RESIN	30.5 μm
4	Laminate	Generic FR-4	304.8 μm
5	SIGNAL	COPPER (80.2%) / COPPER-RESIN	30.5 μm
6	Laminate	Generic FR-4	138.18 μm
7	SIGNAL	COPPER (84.1%) / COPPER-RESIN	50.8 μm
		(a)	

Layer	Density	CTExy	CTEz	Exy	Ez
1	7.3735	24.566	24.566	89,458	89,458
2	1.9000	17.000	70.000	24,804	3,450
3	7.6788	23.173	23.173	94,166	94,166
4	1.9000	17.000	70.000	24,804	3,450
5	7.4942	24.015	24.015	91,319	91,319
6	1.9000	17.000	70.000	24,804	3,450
7	7.7711	22.752	22.752	95,590	95,590
		(b	0)		

Fig. 11. Details of (a) PCB stack-up material and thickness and (b) PCB layer properties.

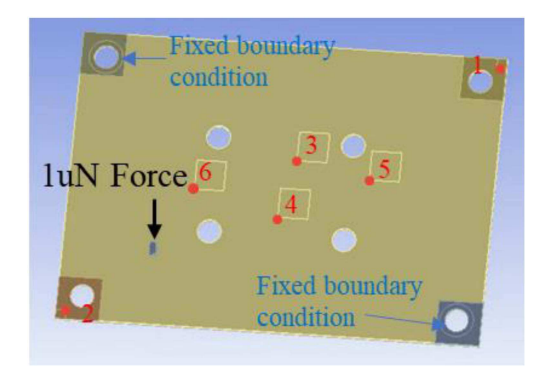


Fig. 12. Simulation model with the same boundary condition and observation points as in the measurement.

The units for the three properties are g/cm^3 , $10^{-6}/^{\circ}C$, and MPa, respectively. The details can be found in Fig. 11.

In the simulation model, on the top left and bottom right corners at the locations of the fixing hole, the circles with the same radius as the screws used in the measurement were set as boundary conditions, as shown in Fig. 12.

The mode resonance frequencies served as one of the criteria to verify the accuracy of the simulation model. From the modal analysis, the simulated PCB self-resonance frequencies are given in Table I. A good correlation verified the model's accuracy. As stated before, the PCB vibration deformation pattern is another criterion. From the corresponding measured and simulated patterns in Figs. 2 and 8, the location of the maximum and minimum deformation, as well as the transition rate achieved consistency. The absolute amplitude of the deformation may not match, because Fig. 8 patterns were excited by the electrical component's force to the PCB in the measurement while Fig. 2 were the self-resonance modes from the simulation thus absolute amplitude was not meaningful.

2.34

Mode	1	2	3	4	5
point 1	2.34	2.08	1.59	1.72	2.59
point 2	2.38	1.89	2.56	2.17	2.54
point 3	2.34	1.91	2.03	1.85	2.38
point 4	1.92	1.84	2.00	1.95	2.64
point 5	2.45	3.2	1.90	1.56	2.02
	2 40	1.00	2.02	1.00	1.00

2.02

TABLE II COIL—MAGNET GENERATED ELECTROMAGNETIC FORCE (μN) EXTRACTED FROM OBSERVATION POINTS

Harmonic response analysis was then performed. Damping ratios for different frequencies were defined in the simulation setting first. The six observation points selected in the measurement were also positioned in the simulation model by using imprinted shapes. A unit force of 1 μ N was applied at the contact surface between the bottom of the capacitor and the board, to represent the force generated by the magnet and coil to the PCB. The contact region was set the same as the 0805 capacitor cross-section size.

The output of the harmonic response analysis was the vibration velocities at the defined observation points that were set at the same location as the measurement. The simulated PCB vibration velocity response at the six observation points is shown in Fig. 13. The numbers noted in the figure are the vibration velocities at the resonance frequencies. A total of six velocity response curves from the six observation points were obtained for the focused modes, which were used as the input for the de-embedding process in the next step.

The system was assumed to be linear, with an external force in the μN range. Consequently, the simulated velocity was proportional to the applied force, and the simulation results with unit force can be used for the de-embedding to obtain the actual force applied to the system.

C. Velocity De-Embedding

Average

The velocity de-embedding is conducted by taking the ratio of the measured velocity excited by the force to be determined and the simulated velocity excited by the 1 μ N force. In Table II, the forces generated by the coil–magnet system at all the observation points for the focused modes are listed.

Some variations were observed for the extracted force caused by the measurement uncertainties described before. After the average force at the six observation points was determined, the variation was effectively removed, so that the extracted force was smooth within the frequency range of interest. The extracted force generated by the coil and magnet with 2 mA input current is shown in Table II and Fig. 14 in blue circles. The averaged force among all the modes is shown in Fig. 14 in blue dashed line.

D. Force Validation

To validate the force extracted by using the proposed methodology, the magnet–coil force was directly simulated in Maxwell

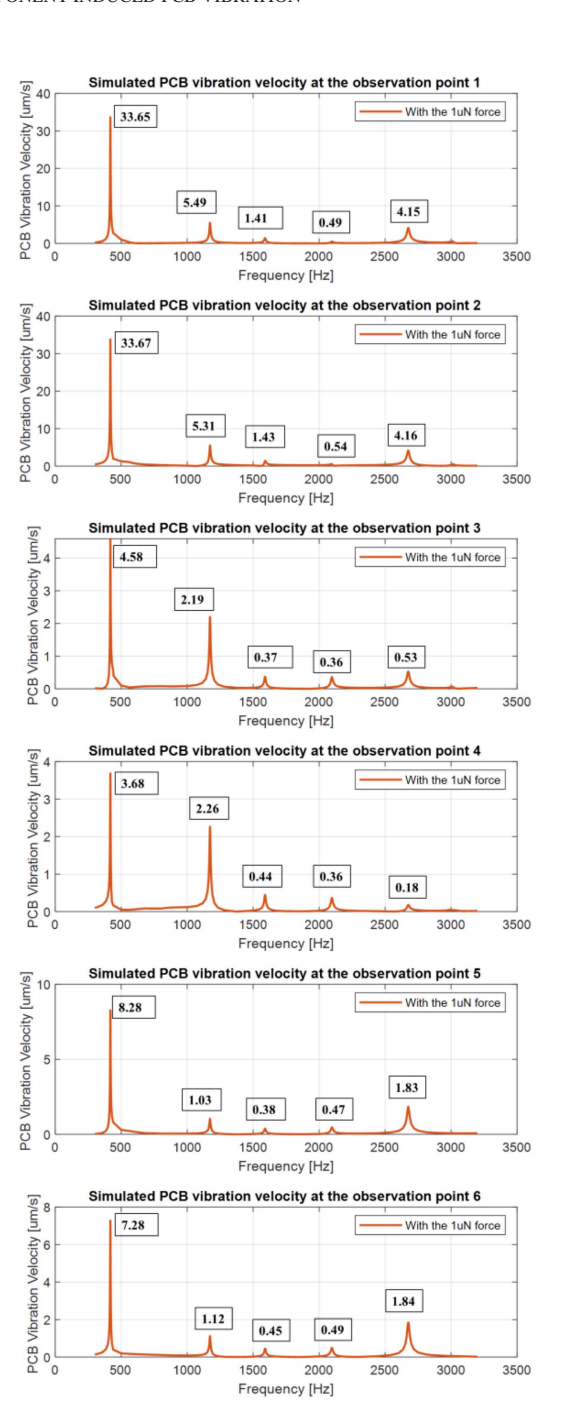


Fig. 13. Simulated PCB vibration velocity at the observation point 1–6. The vibration is excited by the 1 μ N force.

2-D, according to the geometry of the setup. The model was built for half of the cross-section through the center in the x–z plane in Fig. 15(a) and the Maxwell 2-D simulation model is shown in Fig. 15(b). The z-axis represented the center of the coil—magnet system. The center of the magnet and coil was aligned. The magnet was above the coil with the same distance as that in the measurement setup. The number of turns in the upper and lower half of the coil is different and was captured in the model. Current was set to inject into each turn of the coil. The coil input current remained at 2 mA for all frequencies as the measurement, which

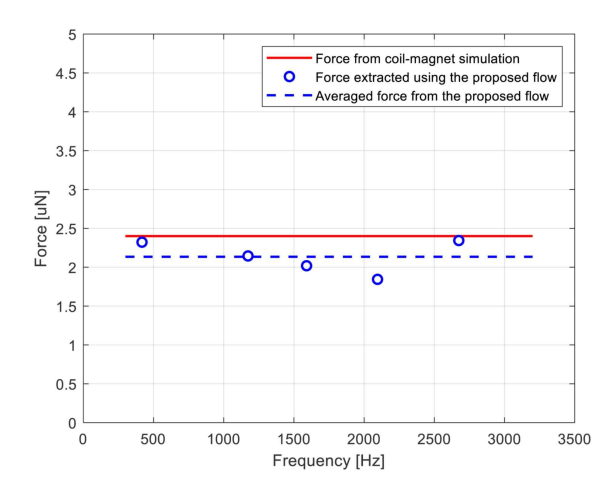


Fig. 14. Comparison between coil—magnet force extracted from the proposed methodology and the simulation.

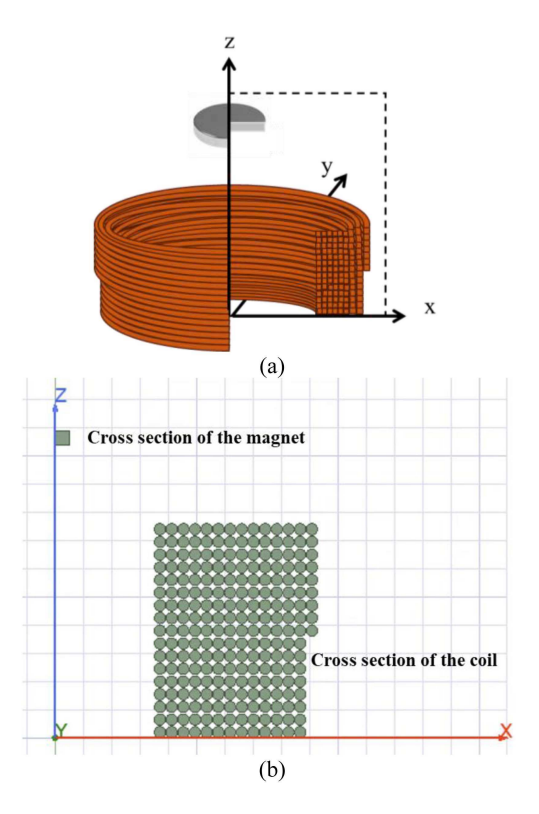


Fig. 15. (a) Coil–magnet system cross-sectional schematic in *x*–*z* plane. (b) Maxwell 2-D simulation model for coil–magnet force extraction.

ideally excited the coil-magnet system for a constant Lorentz force.

The simulated force for the coil–magnet system was approximately 2.4 μ N as shown in Fig. 14 as the red solid line. The averaged force extracted using the proposed methodology is shown as the blue dashed line. Through comparison of the force extracted using the proposed methodology and the force simulated directly according to the setup, a good

correlation was obtained, thereby validating the force extraction methodology.

E. Error Analysis

The discrepancy between the force from the direct simulation and the force extracted by using the proposed flow was 11%, thus indicating a reasonably good match. The errors might have been due to discrepancies between the measurement and simulation setups. For example, a dummy capacitor was placed on the soldering pad between the magnet and the PCB for mechanical support and connection. The mass of the capacitor and the magnet was not included in the simulation due to lightweight. The capacitor might not have been soldered perfectly parallel to the PCB plane, thus causing the oblique of the magnet. Moreover, the centers of the magnet and the coil could not be fully aligned. Therefore, the electromagnetic force acting on the PCB might have had a horizontal component. Force loss might have occurred in transfer from the magnet to the board. Additionally, PCB resonance was used for force extraction. However, resonance characteristics were difficult to fully capture in the simulation. For example, at each resonance frequency, the damping factor calculated from the measurement was applied to the simulation. Any discrepancy between measurement and simulation could propagate and develop to different extents at different resonant frequencies.

V. CONCLUSION

A novel mechanical force extraction methodology for electrical components on PCBs, based on measurement and simulation, is presented herein. The most critical quantity in this process is the PCB vibration at self-resonance frequencies excited by the mechanical force. PCB vibration velocity de-embedding enabled force extraction excluding the test-vehicle effect. An electromagnetic force generated by the mutual effect of a coil and magnet was used for validation of the methodology. The force used for validation was simulated according to the measurement setup and extracted with the proposed methodology. A good correlation between the simulated and extracted force was achieved, with a difference of 11%. The proposed method enables the quantification of the effects of an electrical component, such as an MLCC ("singing" capacitor), on the mechanical performance (vibration) of a PCB.

This method can be directly applied to extract the force induced by electrical components such as an MLCC, and to build the force profile and library, for the system vibration and SPL prediction and correlation. Furthermore, future research may focus on the development of the electrical input and mechanical output transfer function for a given electrical component.

REFERENCES

Y. Guo, D. Kim, Y. Liu, X. Ye, J. Hsu, and J. Fan, "Insertion loss reduction using rounded corners to mitigate surface roughness effect in PCB transmission lines," in *Proc. Asia-Pac. Int. Symp. Electromagn. Compat.*, 2022, pp. 735–738.

- [2] Y. Shim and D. Oh, "Improved PCB via pattern to reduce crosstalk at package BGA region for high speed serial interface," in *Proc. IEEE 64th Electron. Compon. Technol. Conf.*, 2014, pp. 1896–1901.
- [3] G. Ouyang, L. T. Phan, and K. Xiao, "Methods to reduce crosstalk in flex circuit and PCB," in *Proc. IEEE Int. Symp. Electromagn. Compat.*, 2016, pp. 25–28.
- [4] N. Yoshimura and K. Ohnishi, "Impedance control based two-channel architecture in time delayed teleoperation system," in *Proc. IEEE 23rd Int. Symp. Ind. Electron.*, 2014, pp. 1204–1209.
- [5] Y. Ding et al., "Equivalent inductance analysis and quantification for PCB PDN design," in *Proc. IEEE Int. Symp. Electromagn. Compat., Signal Power Integrity*, 2019, pp. 366–371.
- [6] F. D. Paulis et al., "A methodical approach for PCB PDN decoupling minimizing overdesign with genetic algorithm optimization," in *Proc.* IEEE Int. Symp. Electromagn. Compat. Signal/Power Integrity, 2022, pp. 238–243.
- [7] L. Zhang, S. Yong, Y. Liu, and V. Khilkevich, "Auto focus for far field source localization using emission source microscopy," in *Proc. IEEE Int. Joint Electromagn. Compat./Signal Integrity/Power Integrity Electro*magn. Compat. Europe Symp., 2021, pp. 115–118.
- [8] J. Li, V. Khilkevich, R. He, Y. Liu, and J. Zhou, "Imaging distributed sources with sparse ESM technique and Gaussian process regression," in Proc. IEEE Int. Joint Electromagn. Compat./Signal Integrity/Power Integrity Electromagn. Compat. Europe Symp., 2021, pp. 23–28.
- [9] Q. Huang, Y. Liu, L. Li, Y. Wang, C. Wu, and J. Fan, "Radio frequency interference estimation using transfer function based dipole moment model," in *Proc. IEEE Int. Symp. Electromagn. Compat. IEEE Asia-Pac. Symp. Electromagn. Compat.*, 2018, pp. 115–120.
- [10] T. Hatakeyama, R. Kibushi, K. Suzuki, and M. Ishizuka, "Evaluation of heat dissipation performance of printed circuit board using JPCA method in CFD analysis," in *Proc. 13th Int. Microsyst., Packag., Assem. Circuits Technol. Conf.*, 2018, pp. 97–100.
- [11] Y. Chen, "Analysis and research on thermal-force coupling performance of a vehicle controller PCB board," in *Proc. 3rd Int. Conf. Electron Device Mech. Eng.*, 2020, pp. 373–376.
- [12] Y. S. Chen, H. K. Lai, T. C. Lin, P. H. Chang, and M. U. Jen, "Analyses of printed circuit boards subjected to vibration loadings under various clamping types and reinforced ribs," in *Proc. 10th Int. Microsyst., Packag., Assem. Circuits Technol. Conf.*, 2015, pp. 378–381.
- [13] Z. Liu, Y. Sun, and X. Sun, "Fatigue life prediction model for PCB under random vibration," in *Proc. 2nd Int. Conf. Syst. Rel. Saf.*, 2017, pp. 232–237.
- [14] T. Lu, M. Ding, and K. Wu, "Simulation and characterization of singing capacitors in consumer electronics," in *Proc. IEEE Int. Symp. Electromagn. Compat., Signal Power Integrity*, 2019, pp. 522–526.
- [15] Y. Ding et al., "On finding an equivalent force to mimic the multilayer ceramic capacitor vibration," in *Proc. IEEE Symp. Electromagn. Compat. Signal/Power Integrity*, 2023, pp. 120–124.
- [16] A. A. Shabana, Theory of Vibration. Berlin, Germany: Springer-Verlag, 1991
- [17] R. D. Blevins, Formulas for Dynamics, Acoustics and Vibration. Hoboken, NJ, USA: Wiley, 2015.
- [18] J. Xue and R. Diao, "A frequency domain interpolation method for damping ratio estimation," in *Proc. IEEE Int. Conf. Control Syst.*, Comput. Eng., 2014, pp. 251–255.
- [19] U. Zaheer and M. Ajmal, "Comparison of damping estimation techniques for flight tests," in *Proc. 16th Int. Bhurban Conf. Appl. Sci. Technol.*, 2019, pp. 243–247.
- [20] Y. Sun, S. Wu, J. Zhang, C. Hwang, and Z. Yang, "Measurement methodologies for acoustic noise induced by multilayer ceramic capacitors of power distribution network in mobile systems," *IEEE Trans. Electromagn. Compat.*, vol. 62, no. 4, pp. 1515–1523, Aug. 2020.
- [21] Y. Sun, S. Wu, J. Zhang, C. Hwang, and Z. Yang, "Simulation methodologies for acoustic noise induced by multilayer ceramic capacitors of power distribution network in mobile systems," *IEEE Trans. Electromagn. Compat.*, vol. 63, no. 2, pp. 589–597, Apr. 2021.
- [22] X. Yan et al., "A methodology for predicting acoustic noise from singing capacitors in mobile devices," *IEEE Trans. Electromagn. Compat.*, vol. 65, no. 4, pp. 1266–1270, Aug. 2023.



Yifan Ding (Graduate Student Member, IEEE) received the B.S. degree in electrical engineering from Zhejiang University, Hangzhou, China, in 2019. She is currently working toward the Ph.D. degree in electrical engineering with the EMC Laboratory, Missouri University of Science and Technology, Rolla, MO, USA.

Her research interests include system-level power distribution network modeling and design, power supply induced jitter analysis in I/O buffer, and acoustic noise in multilayer ceramic capacitors.



Jianmin Zhang (Senior Member, IEEE) received the B.S. degree from Southeast University, Nanjing, China, and the M.S. and Ph.D. degrees in electrical engineering both from the University of Missouri-Rolla with EMC lab, Rolla, MO, USA, in 2003 and 2007, respectively.

He is currently working with Google, Mountain View, CA, USA, as a Hardware Engineering Manager. Before joining Google, he worked as a SI/PI and RFIC Technical Lead in Apple, an SMTS SI Engineer in Altera Corporation, and a Hardware Technical Lead in

Cisco Systems. His research interests include signal integrity and power integrity for package, PCB and systems, RF desense, coexistence and EMC modeling and analysis, SIP module self-shielding and modeling techniques, singing capacitor source model development, and eNoise modeling and analysis. He has authored and coauthored more than 60 technical papers including journals and conference papers, and reviewed more than 200 academic papers for journals, international conferences and book proposals.

Dr. Zhang was the recipient of the Technical Achievement Award from IEEE EMC Society in 2019 for contributions to the understanding and practice of RF de-sense and co-existence through modeling and measurements, and application in product design, the Conference Best SI Paper Award from the International Microelectronics and Packaging Society in 2007, and the Best Symposium Paper Award and the Best Symposium Student Paper Award both from IEEE EMC Society in 2006. He was the co-advisor of the Best Symposium Student Paper Award from IEEE EMC Society for the year 2018 and 2010. He has served as technical committee members, review board members, session chairs and co-chairs for conferences including IEEE EMC/SIPI Symposium, DesignCon, and EMC Europe etc.



Ming-Feng Xue received the B.S. degree in electronic information engineering from Anhui University, Hefei, China, in 2005, the M.S. degree in electromagnetic field and microwave technology from Shanghai Jiao Tong University, Shanghai, China, in 2008, and the Ph.D. degree in electrical and computer engineering from the University of Illinois at Urbana-Champaign, Urbana, IL, USA, in 2014.

He worked with Apple Inc. as a signal integrity engineer. Since 2021, he has been a Senior Hardware Engineer with Pixel Ecosystem team, Google, Moun-

tain View, CA, USA. His research interests include electromagnetic modeling, multiphysics simulation, and parallel computing.



Xin Hua received the B.S. and M.S. degrees in automotive engineering, and the Ph.D. degree in mechanical engineering from the University of Kentucky, Lexington, KY, USA, in 2013.

He is currently a Hardware Engineer with Google, Mountain View, CA, USA. He worked in the automotive and aerospace industries for about ten years. He specializes in vibro-acoustics with more than 30 publications.



Eric A. MacIntosh (Member, IEEE) received the Bachelor of Science in Engineering from the University of New Brunswick, Fredericton, NB, Canada, in 1999, and the Master of Science degree from Stanford University, Stanford, CA, USA, in 2001, both in electrical engineering.

He is currently a Senior Director of Engineering for Pixel Ecosystem Products with Google, Mountain View, CA. Previously, he was a Senior Engineering Manager with Amazon Lab126 and a Product Engineer for MindTribe and an Engineer with IDEO. His

research interests include wearable computing, audio products, and embedded systems.



Benjamin Leung received the B.S. degree in electrical and computer engineering and computer science from the University of Wisconsin–Madison, Madison, WI, USA, in 1994, and the M.Eng. degree in electrical engineering from Cornell University, Ithaca, NY, USA, in 1996.

He has been working in the design and development of systems in various applications and industries, from telecommunication to consumer products, since 1996. He currently works with Google, Mountain View, CA, USA, focusing on wearables

systems design and development. His current research interests include system miniaturization, system electrical and acoustic noise effects, and RF and antenna miniaturization.



Chulsoon Hwang (Senior Member, IEEE) received the Ph.D. degree in electrical engineering from the KAIST, Daejeon, South Korea, in 2012.

He was a Senior Engineer with Samsung Electronics, Suwon, South Korea, from 2012 to 2015. In 2015, he joined the Missouri University of Science and Technology (formerly University of Missouri-Rolla), Rolla, MO, USA, where he is currently an Associate Professor. His research interests include RF desensitization, signal/power integrity in high-speed digital systems, EMI/EMC, hardware security, and machine

learning.

Dr. Hwang serves as an Associate Editor for IEEE TRANSACTIONS ON SIGNAL AND POWER INTEGRITY. He was a recipient of the AP-EMC Young Scientist Award, the Google Faculty Research Award, and Missouri S&T's Faculty Research Award. He has also been a co-recipient of eight Best/Best Student Paper Awards from various conferences.